Spin inhibition in γ-decay probabilities for states above S_n in Sm and Dy nuclei

C. S. Reingold,[1,2,*] A. Simon,[1,†] R. O. Hughes,[2] J. T. Harke,[2] K. A. Chipps,[3,4] S. Burcher,[4] D. T. Blankstien,[1] J. A. Cizewski,[5] N. Cooper,[1,‡] M. Hall,[1] S. Ota,[6] B. Schroeder,[6] and S. Upadhyayula[6]

[1]*Department of Physics, University of Notre Dame, Notre Dame, Indiana 46556, USA*
[2]*Division of Nuclear and Chemical Sciences, Lawrence Livermore National Laboratory, Livermore, California 94550, USA*
[3]*Physics Division, Oak Ridge National Laboratory, Oak Ridge, Tennessee 37831, USA*
[4]*Department of Physics and Astronomy, University of Tennessee, Knoxville, Tennessee 37996, USA*
[5]*Department of Physics and Astronomy, Rutgers University, New Brunswick, New Jersey 08901, USA*
[6]*Department of Physics and Astronomy, Texas A&M University, College Station, Texas 77843, USA*

(Received 16 December 2020; revised 10 December 2021; accepted 11 February 2022; published 21 March 2022)

When a compound nucleus is formed at an excitation energy above the neutron-separation threshold, it is assumed that its de-excitation will proceed via neutron emission. However, if the excited nucleus is in a high-spin state, but does not have enough excitation energy to conserve angular momentum by either photon emission after neutron emission or relative angular momentum carried off by the neutron, the nucleus will de-excite via γ-emission instead. This effect, the spin inhibition, provides an insight into the structure of the compound nuclei and can aid the understanding of the distribution of the populated spin states in a compound nuclear reaction. In this work, the effects of spin inhibition on the γ-decay probabilities from states in ^{146,147}Sm and ^{160}Dy are presented. For high-spin states above the S_n, spin inhibition is able to suppress neutron emission, and de-excitation via γ-ray emission is observed for states up to 3 MeV above the S_n.

DOI: 10.1103/PhysRevC.105.034612

I. INTRODUCTION

Measuring neutron capture cross sections is necessary for continued understanding of nuclear astrophysics [1,2], as well as nuclear energy [3] and stewardship science applications [4,5]. In many cases, neutron capture cross sections for unstable nuclei are required, which necessitates use of inverse kinematics measurements with radioactive beams. As such, neutron capture reactions cannot be directly measured, since pure neutron targets are not currently available. An alternative approach is to use indirect techniques to determine the neutron capture cross section by measuring a reaction that is experimentally feasible. While the community is preparing for the FRIB-era experiments, it is crucial to benchmark indirect methods for measurements in regular kinematics with stable nuclei and develop a robust understanding of the various techniques.

One of the indirect techniques that can be used is the surrogate method [6,7]. The surrogate reaction method has been used to successfully constrain (n, f) cross sections [8–12]. The method has also been used to constrain radiative capture (n, γ) reactions, but with varying degrees of success [13–15]. One possible explanation for the difficulty the surrogate method has to constrain radiative capture is the discrepancy between the spin distributions populated by the indirect reaction and (n, γ). While research is being conducted to compensate to make surrogate (n, γ) more feasible and repeatable [7,16], there is also insight into the behavior of these systems that can be gleaned from experimental measurements. One phenomenon of particular interest to the surrogate reaction method is the effect of spin-inhibition on the de-exciting compound system [7]. Spin inhibition affects the competition between neutron evaporation and γ-ray emission in a compound system, which will in turn affect the neutron capture cross section. The disparity between the spin distribution occupied by a surrogate reaction and radiative capture must be compensated for during the final cross section calculation. Therefore, the correction for the difference in spin distributions can be significantly impacted by spin inhibition.

Spin inhibition, first introduced by Sperber [17], is the effect where a system is blocked from decay via neutron emission due to angular momentum conservation. In order for a decay via neutron emission to occur in a compound nuclear system, the nucleus must not only be at an appropriate excitation energy, but also spin and parity must be conserved. Therefore, if the excited nucleus is in a high-spin state, but does not have enough excitation energy to conserve angular momentum by either photon emission after neutron emission or relative angular momentum carried off by the neutron, the nucleus cannot undergo de-excitation through the neutron emission channel. Thus the de-excitation proceeds via γ-ray emission. The competition between neutron and γ-ray emission from high-spin states above the S_n has been investigated by several authors [18–20]. In this work, both (p, d) and (p, dn) channels were observed via γ-ray emission; thus,

*reingold1@llnl.gov
†anna.simon@nd.edu
‡Deceased.

the competition can be clearly observed through the change in γ-decay probabilities following both reaction channels.

In compound nuclear reaction theory, it is assumed that the means via which the compound nucleus decays is independent of its formation process, as long as all conservation laws are obeyed [21]. Therefore, studying the competition between neutron emission and γ-decay for a given compound nucleus as a function of excitation energy, spin, and parity can provide insight into the competition between the γ-decay and neutron emission channels. This competition can be studied by measuring the γ-decay probability for transitions between discrete states as a function of nuclear excitation energy around the neutron separation energy S_n. A probe of the competition between neutron and photon emission is the rate at which γ-decay probability drops off as a function of excitation energy after neutron emission becomes energetically viable. Additionally, the spin and parity dependence of the competition can be inferred by measuring the γ-decay probability for transitions between states of various spins and parities.

In this work, (p, d) and (p, t) reactions on self-supporting ^{148}Sm and ^{162}Dy targets were used to determine the γ-decay probabilities for ^{146}Sm, ^{147}Sm, and ^{160}Dy. Additionally, γ rays from the (p, dn) and (p, tn) channels were measured in order to identify the competing neutron-emission channels. Sec II discusses the details of the experimental technique. Sec III provides the details of the analysis procedure. Final results are given in Sec IV where the examples of spin inhibition are presented. The discussion of how the results of this work will inform future calculations of (n, γ) cross sections via the surrogate analysis is given in Sec IV. The complete set of γ-decay probabilities obtained in this work is given in Appendix.

II. EXPERIMENTAL SETUP

The experiment was conducted at the Texas A&M Cyclotron Institute, using the K150 cyclotron. The cyclotron provided a pulsed, 29.55(25) MeV proton beam which was impinged onto self-supported isotopically pure targets of ^{148}Sm and ^{162}Dy. Additionally, ^{208}Pb, mylar, and natural carbon foils were used for detector calibration purposes. The ^{208}Pb(p, d) and ^{12}C(p, d) reactions in these targets provided access to well-separated states in ^{207}Pb and ^{11}C. Access to these states allowed for refined calibrations of the particle detector. Additionally, high-energy γ rays emitted from the $(p, d)\,^{11}$C and $(p, d)\,^{15}$O reactions seen in mylar were used to verify the precision of the HPGe clover calibration over an energy range that would otherwise be inaccessible. Details on these targets can be found in Table I.

The measurements were performed using the Hyperion [22] setup comprised of Compton-suppressed clover detectors for γ-ray measurements and a ΔE-E telescope for particle energy measurements and identification. The silicon telescope employed two double-sided, annular Micron S2 type detectors. The detectors were configured such that there were 24 rings extending out radially and 8 segments perpendicular to both the radial and beam axes. The thickness of the S2 detectors was 150 μm and 1.5 mm for the ΔE and $E1$ detector, respectively. This configuration was selected to maximize the separation between incident protons, deuterons, and tritons, as well as ensure that all deuterons and tritons of interest were fully stopped in the telescope. An example of the separation achieved with this configuration can be found in the particle identification (PID) plot in Fig. 1(a). PID gates were imposed on the data as a function of linearized PID, R, which was defined as

$$R(E_{\Delta E}, E_{E1}) = (E_{\Delta E} + E_{E1})^{1.67} - E_{E1}^{1.67}\cos\theta. \quad (1)$$

The telescope was placed 18 mm downstream of the target, covering projectile recoil angles θ in the range 35–60° in the laboratory frame. The coincidence gates shown in Fig. 1(a) were selected to exclude the overlap regions in the PID plot and avoid mixing of the reaction channels. A typical particle spectrum taken with the S2 telescope can be found in Fig. 1(c).

For this experiment, an array of nine clover detectors with BGO Compton suppression shields was used. The detectors were placed at 35°, 90°, and 135° in respect to the beam direction. The BGO shields were comprised of 16 optically isolated BGO crystals, each with a dedicated PMT. The PMTs of each shield were daisy-chained to provide a single veto channel. The HPGe clover detectors were comprised of four, tightly packed, electrically isolated, 5 cm × 5 cm × 8 cm germanium crystals, each with an individual readout. Add-back between the four crystals was performed offline for event reconstruction of Compton scattered γ rays that were fully absorbed within the detector. Events that were not fully absorbed were vetoed offline using the BGO shields as an anticoincidence gate. Sample γ-ray spectra taken with Hyperion can be found in Fig. 1(d).

TABLE I. Properties of the target foils that were used in this work.

Target	Thickness (mg/cm^2)	Enrichment
^{148}Sm	1.10(6)	98(2)%
^{162}Dy	0.85(4)	98(2)%
^{208}Pb	1.83(9)	97(3)%
^{12}C	0.100(5)	natural
Mylar	0.345(17)	–

III. ANALYSIS

The analysis procedure followed the standard procedure for the Hyperion array. The leaves of the HPGe clover detectors were individually calibrated using several standard calibration sources. The ΔE and $E1$ detectors were calibrated using a ^{226}Ra source and known levels in ^{207}Pb and ^{11}C, which were accessed through the (p, d) reaction channels on target materials listed in Table I. In order to account for energy losses in the dead layers of the telescope, energy loss in aluminum and gold dead layers on the front and back of the S2 detectors was calculated using the energy loss calculator ELAST.

Since this analysis requires measuring γ-ray intensities as a function of nuclear excitation energy, finalized particle energies had to be recoil corrected to determine the excitation energy from which they originated. The non-relativistic recoil

correction for an arbitrary reaction $X(a, b)Y$ is given by

$$E_{ex}(T_a, T_b, \theta) = Q - \frac{1}{m_Y}[(m_Y + m_b)T_b - (m_Y - m_a)T_a - 2\sqrt{m_a m_b T_a T_b}\cos\theta]. \quad (2)$$

The masses, m_a, m_b, and m_Y, and Q values for the reactions studied in this work are well known, and the kinetic energy of the beam particles T_a are calculated from the cyclotron frequency. Therefore, the only measured quantities necessary to calculate the nuclear excitation energy via recoil correction are the kinetic energy T_b and recoil angle θ of the reaction ejectile b. The segmentation of the S2 detectors, allows for simultaneous measurement of both T_b and θ in the telescope.

The particle-γ coincidence events for each of the reaction channels were converted into E_{ex}-E_γ matrices, as shown in Fig. 1(b). Random coincidences were subtracted from the matrices based on the particle-γ timing information. Data from all of the clovers were combined into one matrix for each of the reactions.

Since the expected intrinsic efficiency of the silicon relative to the clovers is nearly 100%, the γ-ray efficiency $\varepsilon_\gamma(E_\gamma)$ is effectively the total Hyperion efficiency. The efficiency of Hyperion was determined through a combination of data from standard γ-ray sources, ^{60}Co, ^{137}Cs, and ^{152}Eu, and simulation. A GEANT4 [23] simulation was used to extend the efficiency curve beyond 1.5 MeV range covered by the source data. The simulation was designed to contain all of the detectors present in the experiment, as well as the BGO hevimets, target ladder, chamber, and internal components of the chamber. As shown in Fig. 2 for the example of ^{60}Co, a very good agreement was obtained between the simulation and experimental data.

In order to assess the accuracy of the simulation, a histogram of the residual differences between the measured and simulated spectra was generated. In Fig. 2, the result for ^{60}Co is shown. The residuals follow a Gaussian distribution, centered about zero with a width (σ) of 43 counts. The width of this distribution was used to estimate a 1σ width of the photopeak efficiency curve obtained from the simulation. The simulated photopeak efficiency is compared to the measured efficiencies obtained for the γ calibration sources. A very good agreement between the simulation and measurement was obtained, as shown in Fig. 3.

Finally, the simulation was used to determine the total efficiency of the Hyperion array. All nine clovers were simulated at their respective positions in the array. The uncertainty of the simulated efficiency for each clover was propagated to the final efficiency. The final efficiency of the Hyperion array was determined to be 0.2(1)% at 1.33 MeV.

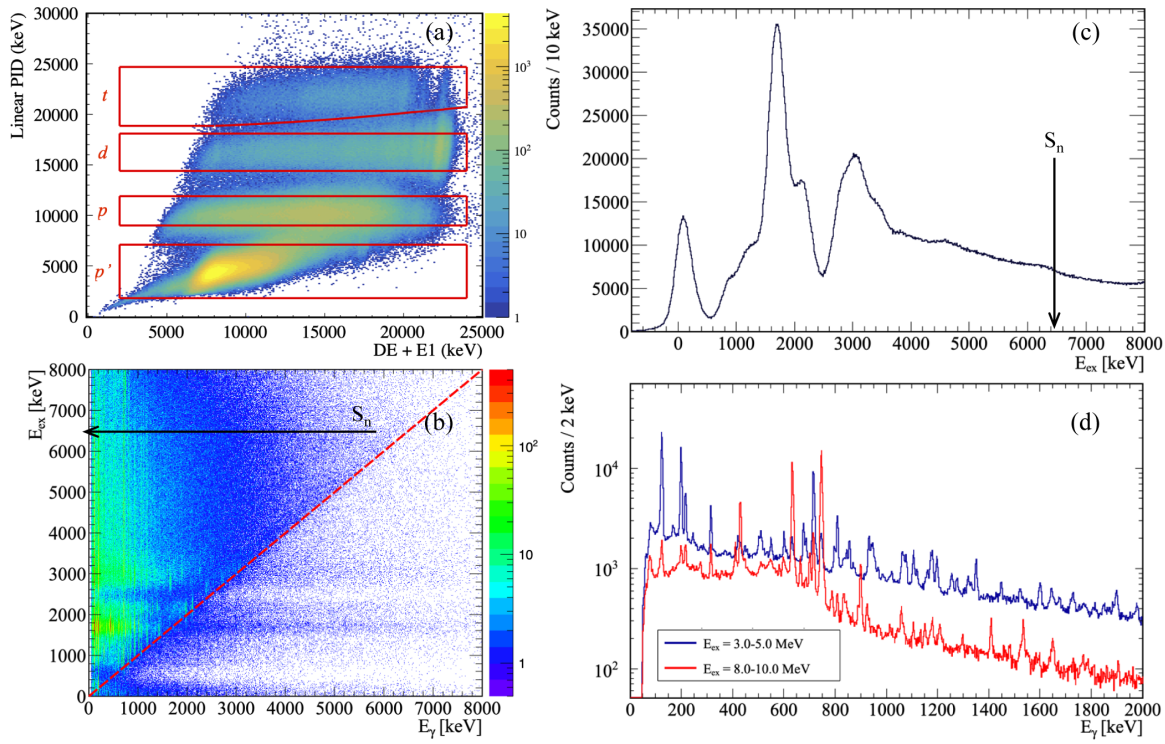

FIG. 1. Example experimental data obtained from the ^{148}Sm(p, d) ^{147}Sm reaction measured with Hyperion: (a) Linearized particle identification (PID) plot used to select the (p,d) reaction that populates ^{147}Sm nucleus. Red contours denote coincidence gates applied to select protons, deuterons and tritons in the outgoing particle channel. (b) E_{ex}-E_γ matrix. The red dashed line denotes $E_{ex} = E_\gamma$. Discrete transitions appear to dominate below about 3.5 MeV, after which point the γ-decay seems to follow a probabilistic, continuous behavior. The arrow indicates the neutron-separation energy in ^{147}Sm. (c) Particle singles spectrum for (p, d) ^{147}Sm channel. The arrow indicated the neutron-separation energy in ^{147}Sm. (d) γ-ray spectrum from the ^{148}Sm(p, d) reaction. The blue histogram shows γ-ray transitions in coincidence with excitation energies between 3.0-5.0 MeV, where only the (p, d) channel is present. The red histogram represents γ-ray transitions in coincidence with excitation energies between 8.0-10.0 MeV, where both the (p, d) and (p, dn) channels are open.

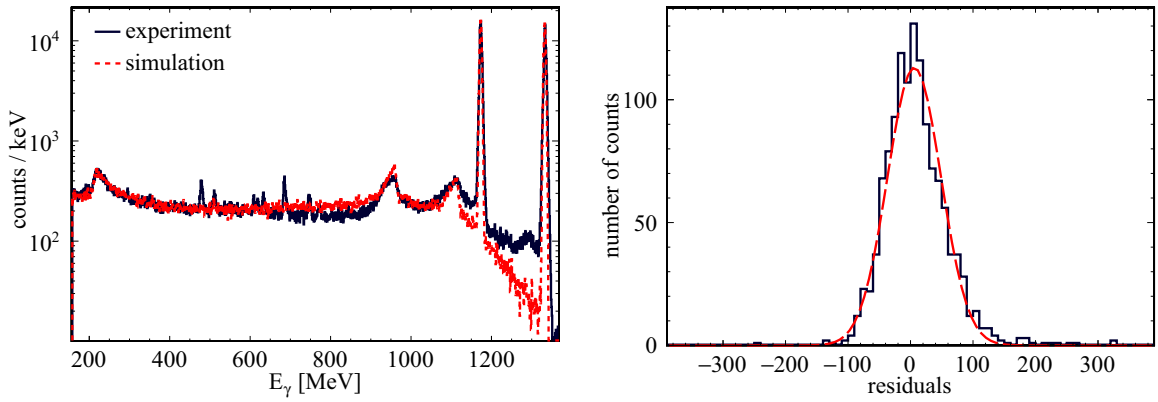

FIG. 2. (Left) A comparison between the GEANT4 simulation (red dashed line) and measured spectra (black) for ^{60}Co. The differences in the spectra are primarily due to contaminants that were present in the singles spectra. (Right) A histogram of residual differences between between the measured ^{60}Co spectrum and a simulated one. A Gaussian fit (red dashed line) was used to determine the width of the distribution.

IV. γ-DECAY PROBABILITIES

The γ-decay probabilities measured in this work are defined as follows:

$$P_{\delta\gamma}(E_{ex}) = \frac{N_{\delta\gamma}(E_{ex})}{N_{\delta}(E_{ex})\varepsilon_{\gamma}(E_{\gamma})}, \tag{3}$$

where $N_{\delta\gamma}$ is the number of particle-γ coincidences, N_{δ} is the total number of particle singles, and ε_{γ} the γ-ray efficiency.

Since the quantity of interest was the γ-decay probability as a function of excitation energy, horizontal projections of the coincidence matrix were generated in 100–200 keV steps around S_n for an energy range between $S_n - 2$ MeV to $S_n + 4$ MeV. The width of these steps was varied to accommodate the available statistics in the matrix.

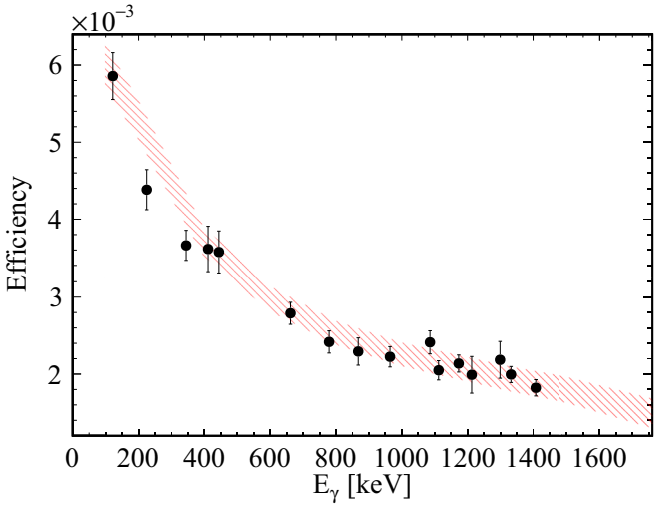

FIG. 3. A comparison between the photopeak efficiency extracted from the simulation and from source data, both for a single clover. Sources used for this figure are ^{152}Eu, ^{137}Cs, and ^{60}Co. Each data point represents the photopeak efficiency for a γ-ray energy for a given source. The red band represents the simulated efficiency and its 1σ uncertainty band.

The $N_{\delta\gamma}$ was determined by integrating the γ-ray line of interest for each E_{ex} bin. The width of the γ-ray lines was determined by a Gaussian fit to the γ-ray peak and the obtained 3σ range was used for each excitation energy bin to ensure consistency in the analysis. The Compton background under the peak was determined for each E_{ex} bin from a linear fit to the γ-ray spectrum near the line of interest. The total number of decays for a given excitation energy bin, N_{δ}, was obtained by integration of the total spectrum of the particle singles within the same energy bin of 100–200 keV.

The measured γ-decay probabilities for the transitions between the first three states in ^{147}Sm are displayed in Fig. 4. For excitation energies below the S_n, the neutron emission channel is closed, thus the de-excitation proceeds through γ-ray emission. The decay probabilities remain relatively constant. Once the nucleus is excited above S_n, neutron emission is expected to become the primary method of de-excitation. Therefore, the probability of de-excitation via emission of γ rays from the residual nucleus rapidly decreases. This behavior can be observed for decay via the 121.2 keV and 197.3 keV lines that correspond to the transitions between the lowest two excited states in ^{147}Sm. However, the probability of de-excitation from the continuum through the third transition, corresponding to the γ ray at $E_{\gamma} = 716.6$ keV, does not begin to fall off until an excitation energy much larger than S_n is reached. This behavior is a product of spin inhibition [17].

Since the spin and parity of the third excited state of ^{147}Sm is $(11/2)^{-}$, it can be assumed that reactions that excite the compound ^{147}Sm nucleus into high-spin states will undergo photon emission to this relatively high-spin state. That is, until a high-spin state in ^{146}Sm becomes energetically available. The excitation energy at which the 716.6 keV γ ray begins to turn off corresponds to S_n plus the energy of the second excited state in ^{146}Sm. At this point, the emission of 430.4 keV γ ray in ^{146}Sm is observed, indicating that the neutron emission following the (p, d) channel is now open.

This process can be further verified by observation of the γ-decay probabilities of the ^{146}Sm compound nucleus that results from (p, dn) reaction channel. As shown in Fig. 5,

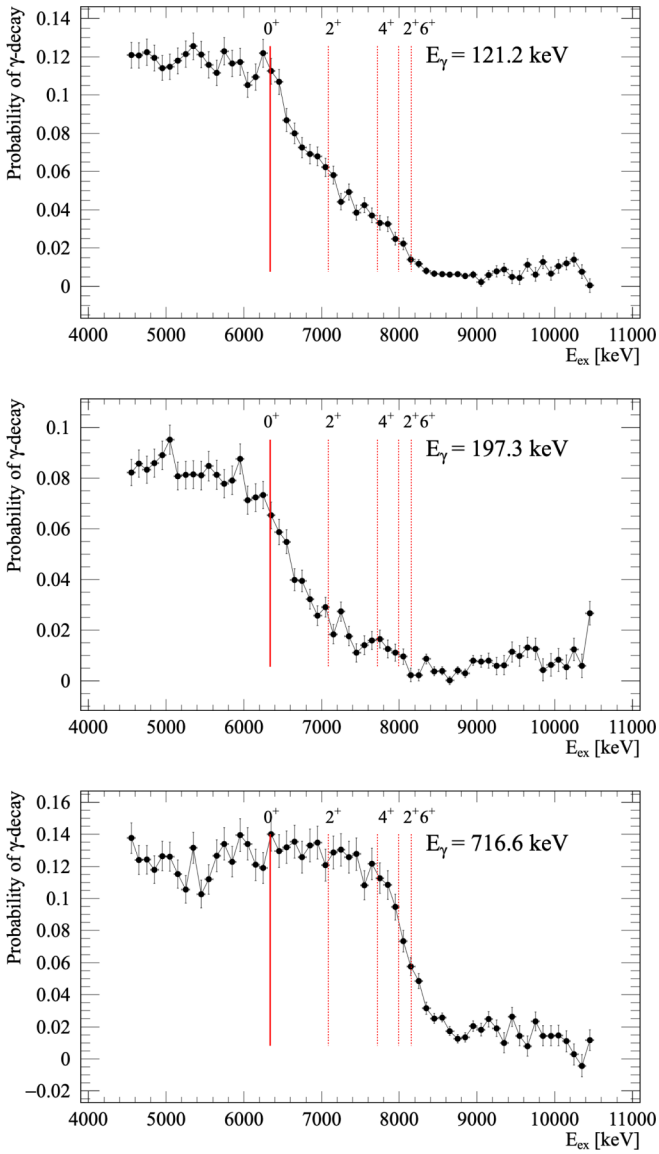

FIG. 4. Extracted γ-decay probabilities for the first three transitions in ^{147}Sm, via the (p, d) reaction channel. The solid line denotes the neutron separation energy S_n, and the dotted lines correspond to the energies of the first few discrete states in ^{146}Sm. The spins and parities of the ^{146}Sm levels are noted on the figure.

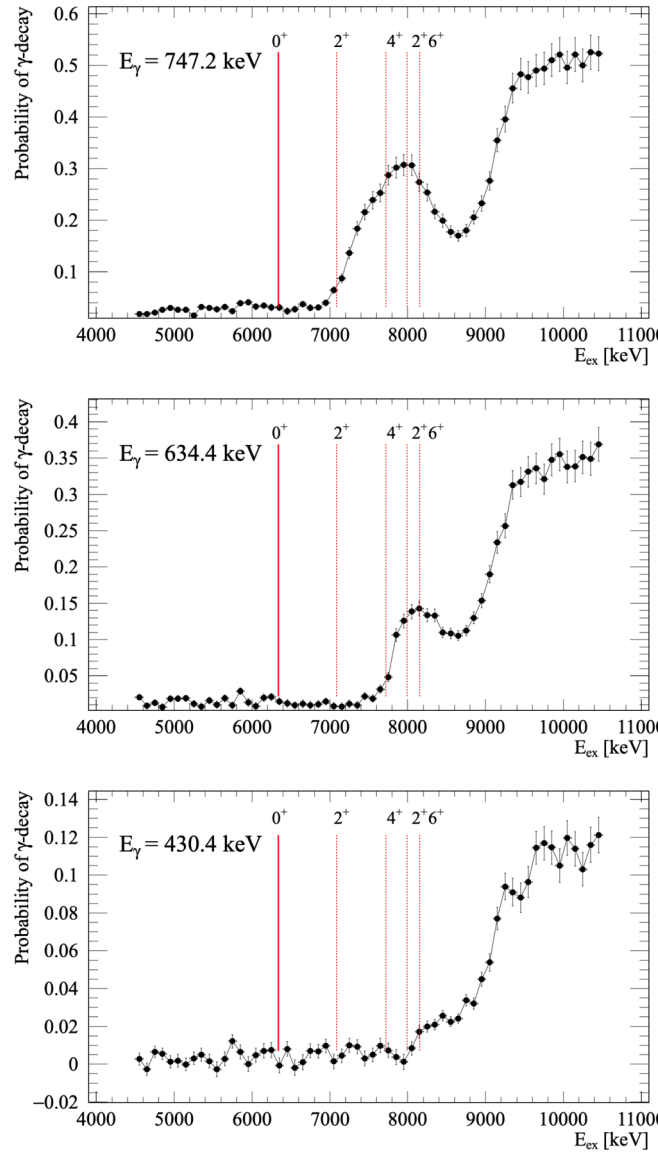

FIG. 5. Extracted γ-decay probabilities for the first three transitions in ^{146}Sm, via the (p, dn) reaction channel. The solid line denotes the neutron separation energy S_n, and the dotted lines correspond to the energies of the first few discrete states in ^{146}Sm. The spins and parities of the ^{146}Sm levels are noted on the figure.

the γ-decay probabilities in this nucleus exhibit the opposite trend. At excitation energies below the S_n, when the (p, dn) channel is closed, the γ-decay probabilities are consistent with zero and immediately increase once excited states above the S_n are populated. However, in case of the decay via $E_\gamma =$ 430.4 keV, the probabilities pick up at energies nearly 2 MeV above the S_n, at which a high-spin state in ^{146}Sm is available for neutron emission.

In total, 16 transitions in ^{147}Sm (Table II), ^{146}Sm (Table III) and ^{160}Dy (Table IV) were extracted. All the results are compiled in the Appendix. In the case of transitions originating from high-spin states, the spin inhibition can be observed. For some of the transitions, probabilities greater than 1.0 are reported in the Appendix. This is due to the definition of

TABLE II. Measured transitions for ^{147}Sm.

γ-ray	Initial state		Final state	
(keV)	(keV)	J^π	(keV)	J^π
121.2	121.2	$5/2^-$	0.0	$7/2^-$
197.3	197.3	$3/2^-$	0.0	$7/2^-$
215.3	932.0	$11/2^+$	716.6	$11/2^-$
314.3	1030.7	$13/2^+$	716.6	$11/2^-$
716.6	716.6	$11/2^-$	0.0	$7/2^-$
809.4	809.4	$9/2^-$	0.0	$7/2^-$

TABLE III. Measured transitions for ^{146}Sm.

γ-ray	Initial state		Final state	
(keV)	(keV)	J^π	(keV)	J^π
410.8	2222.4	6^+	1811.7	6^+
430.4	1811.7	6^+	1381.3	4^+
634.1	1381.3	4^+	747.2	2^+
702.1	2083.4	5^-	1381.3	4^+
747.2	747.2	2^+	0.0	0^+
900.8	1648.0	2^+	747.2	2^+

the decay probability give by Eq. (3), where multiple decay branches that proceed via given γ-ray transition are combined into one probability plot.

V. DISCUSSION

Particle-γ matrices for ^{146}Sm, ^{147}Sm, and ^{160}Dy were measured using the Hyperion detector array, and γ-decay probabilities were extracted from these matrices. While some γ rays behaved as expected, by becoming less probable immediately after the excitation energy exceeded S_n, other γ rays exhibited a phenomenon known as spin inhibition. These states are likely being fed from high-spin states in the continuum, where angular momentum conservation prohibits de-excitation by neutron emission.

Experimental evidence of these high-spin continuum states feeding discrete, high spin states in the compound system of interest further supports the claims of Escher *et al.* [6] that the Weisskopf-Ewing approximation is an inappropriate assumption to make while determining the (n, γ) surrogate cross section. The Weisskopf-Ewing approximation assumes the decay probability for a compound system will be independent of spin and parity. This behavior, however, is only expected for spins significantly lower than the spin-cutoff parameter [24]. Previous experiments have shown the perils of using the Weisskopf-Ewing approximation when attempting a surrogate (n, γ) cross section measurement. Scielzo *et al.* [13] observed an overestimation of the ^{155,157}Gd(n, γ) cross sections by a factor of 2–3.4 when the Weisskopf-Ewing approach was utilized. Other experiments [14,15] have also shown results consistent with those presented in Ref. [13]. Ota *et al.* [20] were able to extract γ-decay probabilities for ^{90}Zr using (p, p'), (p, d), and (p, t) reactions. In spite of their experimental success, they stopped their efforts just short of determining the neutron capture cross section ^{89}Zr(n, γ) since the surrogate method was underdeveloped for (n, γ) at the time of their publication. Therefore, experimental evidence of spin inhibition in the samarium and dysprosium isotopes studied here clearly show that the implementation of the Weisskopf-Ewing approximation will significantly overestimate the (n, γ) cross sections for these isotopes.

TABLE IV. Measured transitions for ^{160}Dy.

γ-ray	Initial state		Final state	
(keV)	(keV)	J^π	(keV)	J^π
86.8	86.8	2^+	0.0	0^+
197.0	283.8	4^+	86.8	2^+
297.2	581.1	6^+	283.8	4^+
385.7	966.9	8^+	581.1	6^+

Given the overwhelming evidence against performing a surrogate cross section calculation without an appropriate spin distribution, we have elected not to include a cross section in this work. Utilization of the measured γ-decay probabilities presented in this work to constrain (n, γ) cross sections requires a formation probability of the compound nucleus in the (p, d) reaction to be calculated. The work by Potel *et al.* [25] realized that the non-elastic breakup of the weakly bound deuteron provides a channel for the compound nucleus to be formed in the (d, p) reaction. Subsequently, Ratkiewicz *et al.* [26] used the Potel calculated (p, d) entry J^π distributions for the surrogate compound nucleus to deduce (n, γ) cross sections that are well reproduced by previous measurements and evaluations. Analogous theoretical advancements are needed to calculate (p, d) entry J^π distributions for the surrogate compound nucleus beyond the work of Escher *et al.* [7] for $A \approx 90$ nuclei and that takes into account multistep processes. Although an accurate calculation is inaccessible at the time of publication, further development of the surrogate method will inevitably provide the means for generating the formation probability of the compound nucleus for the rare earth elements studied in this work. Progress is constantly being made to reconcile the different spin distributions populated by charged particle transfer reactions and neutron capture [7]. Therefore, the authors of this work are confident a method to perform surrogate neutron capture cross section calculations with rare earth elements will become available in the near future.

Once the formation probability becomes available, the results of this work will provide a comparison between the surrogate method and the Oslo method [27–29], another indirect technique for (n, γ) measurements. Several measurements of neutron capture cross sections for Sm nuclei obtained using the Oslo method have already been published [30] including ^{146}Sm discussed in this work. The Oslo analysis of the data utilized in this work is currently ongoing. Additionally, with scarce (n, γ) cross section data for ^{145}Sm and no data for ^{146}Sm available via the EXFOR database [31], the indirect measurements will provide the first insight into the neutron capture cross sections for these nuclei.

ACKNOWLEDGMENTS

This work was supported by the U.S. Department of Energy No. DE-NA0003780, No. DEFG02-95ER-40934, and No. DE-NA0003841, DOE NNSA Grant No. DE-NA0000979, National Science Foundation PHY-1404218 and PHY-1713857, and by Lawrence Livermore National Laboratory under Contract No. DE-AC52-07NA27344.

APPENDIX: γ-DECAY PROBABILITIES

Figures 6–8 show all the γ-decay probabilities extracted within this work for ^{146,147}Sm and ^{160}Dy.

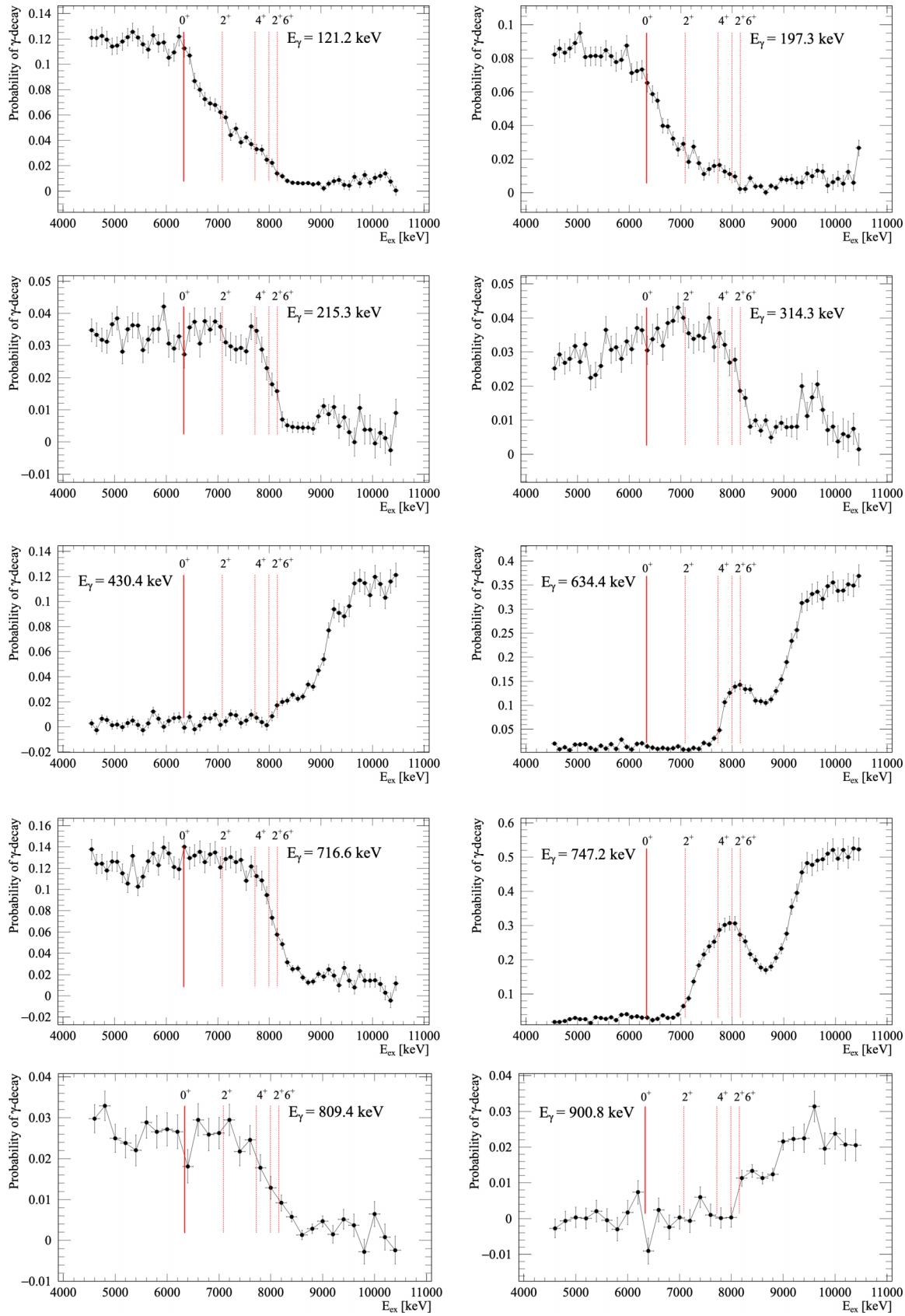

FIG. 6. Extracted γ-decay probabilities for the transitions in ^{147}Sm, via the (p, d) reaction channel. The solid line denotes the neutron separation energy S_n, and the dotted lines correspond to the energies of the first few discrete states in ^{146}Sm. The spins and parities of the ^{146}Sm levels are noted on the figure. Transitions via 430.4, 634.4, 747.2 and 900.8 keV γ rays correspond to ^{146}Sm and demonstrate the spin inhibition after neutron emission.

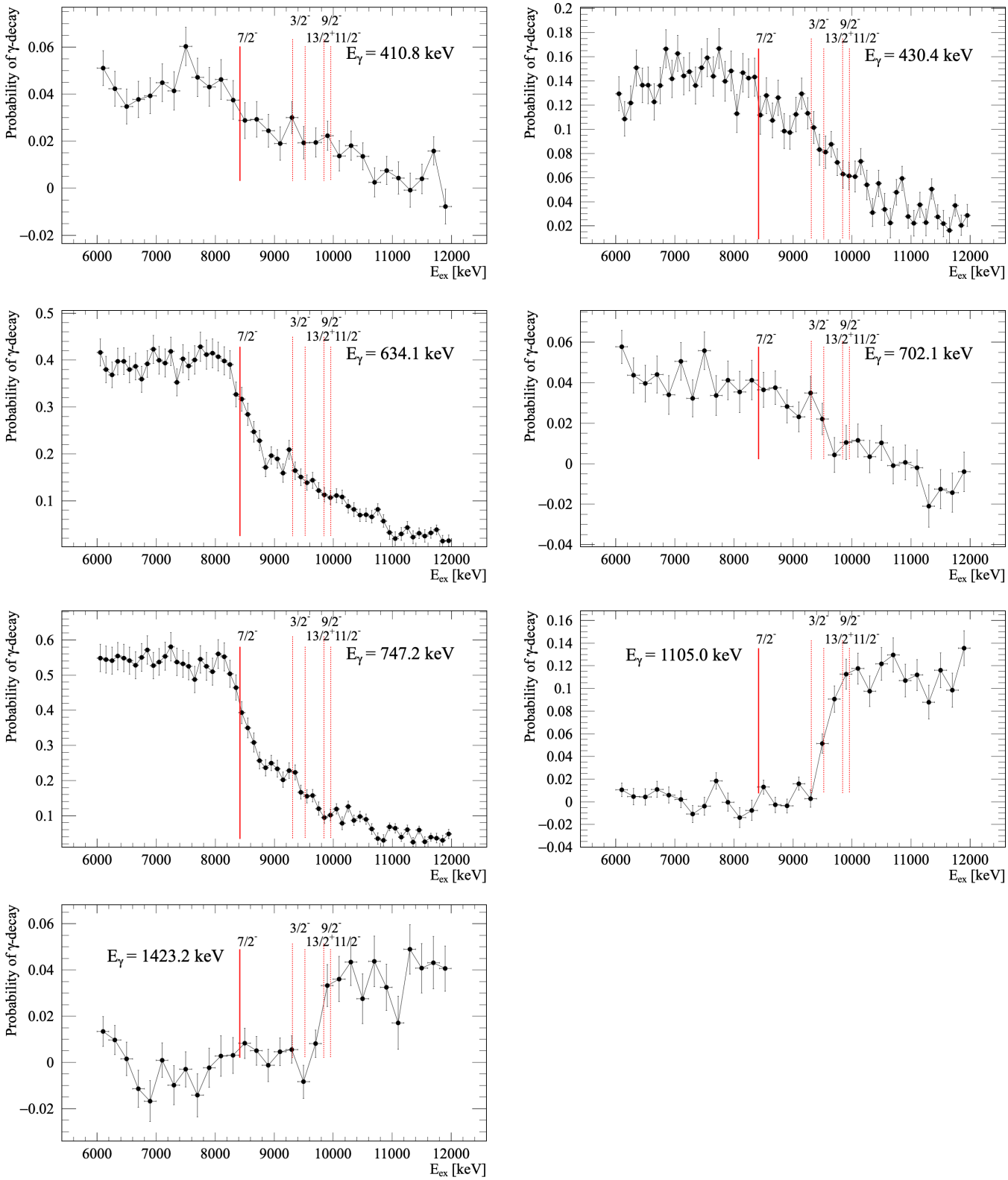

FIG. 7. Extracted γ-decay probabilities for the transitions in ^{146}Sm, via the (p,t) reaction channel. The solid line denotes the neutron separation energy S_n, and the dotted lines correspond to the energies of the first few discrete states in ^{145}Sm. The spins and parities of the ^{145}Sm levels are noted on the figure. Transitions via 1105.0 and 1432.2 keV γ rays correspond to ^{145}Sm and demonstrate the spin inhibition after neutron emission.

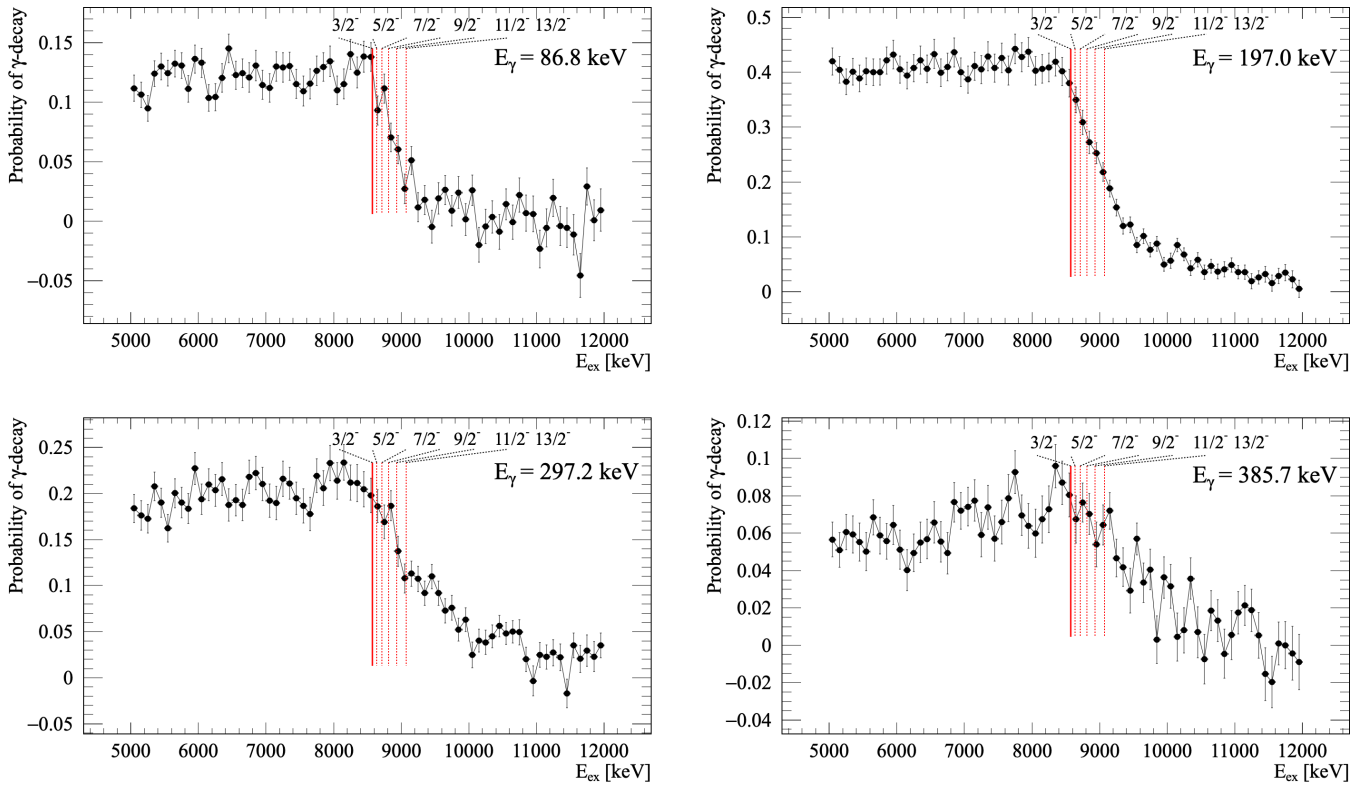

FIG. 8. Extracted γ-decay probabilities for the transitions in ^{160}Dy, via the (p, t) reaction channel. The solid line denotes the neutron separation energy S_n, and the dotted lines correspond to the energies of the first few discrete states in ^{159}Dy. The spins and parities of the ^{159}Dy levels are noted on the figure.

[1] T. Rauscher, P. Mohr, I. Dillmann, and R. Plag, Opportunities to constrain astrophysical reaction rates for the *s*-process via determination of the ground-state cross-sections, Astrophys. J. **738**, 143 (2011).

[2] F. Käppeler, R. Gallino, S. Bisterzo, and W. Aoki, The *s* process: Nuclear physics, stellar models, and observations, Rev. Mod. Phys. **83**, 157 (2011).

[3] N. Colonna, F. Belloni, E. Berthoumieux, M. Calviani, C. Domingo-Pardo, C. Guerrero, D. Karadimos, C. Lederer, C. Massimi, C. Paradela, R. Plag, J. Praena, and R. Sarmento, Advanced nuclear energy systems and the need of accurate nuclear data: The n_TOF project at CERN, Energy Environ. Sci. **3**, 1910 (2010).

[4] M. May, Nuclear forensics: Role, state of the art, program needs, technical report, nuclear forensics working group of the American Physical Society's panel on public affairs and the American Association for the Advancement of Science (2008).

[5] M. Kreisler, National nuclear security and other applications of Rare Isotopes, in *Proceedings of Particle Accelerator Conference (PAC)* (IEEE, Piscataway, NJ, 2007).

[6] J. E. Escher, J. T. Harke, F. S. Dietrich, N. D. Scielzo, I. J. Thompson, and W. Younes, Compound-nuclear reaction cross sections from surrogate measurements, Rev. Mod. Phys. **84**, 353 (2012).

[7] J. E. Escher, J. T. Harke, R. O. Hughes, N. D. Scielzo, R. J. Casperson, S. Ota, H. I. Park, A. Saastamoinen, and T. J. Ross, Constraining Neutron Capture Cross Sections for Unstable Nuclei with Surrogate Reaction Data and Theory, Phys. Rev. Lett. **121**, 052501 (2018).

[8] W. Younes and H. C. Britt, Neutron-induced fission cross sections simulated from (t, pf) results, Phys. Rev. C **67**, 024610 (2003).

[9] J. E. Escher and F. S. Dietrich, Determining (n, f) cross sections for actinide nuclei indirectly: Examination of the surrogate ratio method, Phys. Rev. C **74**, 054601 (2006).

[10] G. Kessedjian, B. Jurado, M. Aiche, G. Barreau, A. Bidaud, S. Czajkowski, D. Dassié, B. Haas, L. Mathieu, L. Audouin, N. Capellan, L. Tassan-Got, J. Wilson, E. Berthoumieux, F. Gunsing, C. Theisen, O. Serot, E. Bauge, I. Ahmad, J. Greene *et al.*, Neutron-induced fission cross sections of short-lived actinides with the surrogate reaction method, Phys. Lett. B **692**, 297 (2010).

[11] J. J. Ressler, J. T. Harke, J. E. Escher, C. T. Angell, M. S. Basunia, C. W. Beausang, L. A. Bernstein, D. L. Bleuel, R. J. Casperson, B. L. Goldblum, J. Gostic, R. Hatarik, R. Henderson, R. O. Hughes, J. Munson, L. W. Phair, T. J. Ross, N. D. Scielzo, E. Swanberg, I. J. Thompson *et al.*, Surrogate measurement of the ^{238}Pu(n, f) cross section, Phys. Rev. C **83**, 054610 (2011).

[12] R. J. Casperson, J. T. Harke, N. D. Scielzo, J. E. Escher, E. McCleskey, M. McCleskey, A. Saastamoinen, A. Spiridon, A. Ratkiewicz, A. Blanc, M. Kurokawa, and R. G. Pizzone,

Measurement of the ^{240}Am(n, f) cross section using the surrogate-ratio method, Phys. Rev. C **90**, 034601 (2014).

[13] N. D. Scielzo, J. E. Escher, J. M. Allmond, M. S. Basunia, C. W. Beausang, L. A. Bernstein, D. L. Bleuel, J. T. Harke, R. M. Clark, F. S. Dietrich, P. Fallon, J. Gibelin, B. L. Goldblum, S. R. Lesher, M. A. McMahan, E. B. Norman, L. Phair, E. Rodriquez-Vieitez, S. A. Sheets, I. J. Thompson *et al.*, Measurement of γ-emission branching ratios for ^{154,156,158}Gd compound nuclei: Tests of surrogate nuclear reaction approximations for (n, γ) cross sections, Phys. Rev. C **81**, 034608 (2010).

[14] T. J. Ross, C. W. Beausang, R. O. Hughes, J. M. Allmond, C. T. Angell, M. S. Basunia, D. L. Bleuel, J. T. Harke, R. J. Casperson, J. E. Escher, P. Fallon, R. Hatarik, J. Munson, S. Paschalis, M. Petri, L. Phair, J. J. Ressler, N. D. Scielzo, and I. J. Thompson, Measurement of the entry-spin distribution imparted to the high excitation continuum region of gadolinium nuclei via (p, d) and (p, t) reactions, Phys. Rev. C **85**, 051304(R) (2012).

[15] G. Boutoux, B. Jurado, V. Méot, O. Roig, L. Mathieu, M. Aïche, G. Barreau, N. Capellan, I. Companis, S. Czajkowski, K.-H. Schmidt, J. Burke, A. Bail, J. Daugas, T. Faul, P. Morel, N. Pillet, C. Théroine, X. Derkx, O. Sérot *et al.*, Study of the surrogate-reaction method applied to neutron-induced capture cross sections, Phys. Lett. B **712**, 319 (2012).

[16] N. Cooper, C. W. Beausang, P. Humby, A. Simon, J. T. Harke, R. O. Hughes, S. Ota, C. Reingold, A. Saastamoinen, and E. Wilson, Entry-level spin distributions and relative γ-neutron branching ratios of samarium isotopes populated by the (p, t) reaction, Phys. Rev. C **98**, 044618 (2018).

[17] D. Sperber, Competition between neutron and gamma emission from nuclear states with high spin, Phys. Rev. **141**, 927 (1966).

[18] D. Sarantites and B. Pate, Angular momentum effects in the compound-statistical model for nuclear reactions: (I). Monte Carlo calculations of excitation functions, Nucl. Phys. A **93**, 545 (1967).

[19] C. Ling, D. Bodansky, J. R. Calarco, and J. M. Cameron, Neutron-gamma competition following (d, d') reactions, Phys. Rev. C **5**, 1622 (1972).

[20] S. Ota, J. T. Harke, R. J. Casperson, J. E. Escher, R. O. Hughes, J. J. Ressler, N. D. Scielzo, I. J. Thompson, R. A. E. Austin, B. Abromeit, N. J. Foley, E. McCleskey, M. McCleskey, H. I. Park, A. Saastamoinen, and T. J. Ross, Spin differences in the ^{90}Zr compound nucleus induced by(p, p'),(p, d), and (p, t) surrogate reactions, Phys. Rev. C **92**, 054603 (2015).

[21] N. Bohr, Neutron capture and nuclear constitution, Nature (London) **137**, 344 (1936).

[22] R. Hughes, J. Burke, R. Casperson, S. Ota, S. Fisher, J. Parker, C. Beausang, M. Dag, P. Humby, J. Koglin, E. McCleskey, A. McIntosh, A. Saastamoinen, A. Tamashiro, E. Wilson, and T. Wu, The Hyperion particle-γ detector array, Nucl. Instrum. Methods Phys. Res. A **856**, 47 (2017).

[23] S. Agostinelli, J. Allison, K. Amako, J. Apostolakis, H. Araujo, *et al.*, Geant4—a simulation toolkit, Nucl. Instrum. Methods Phys. Res. A **506**, 250 (2003).

[24] J. E. Escher and F. S. Dietrich, Cross sections for neutron capture from surrogate measurements: An examination of Weisskopf-Ewing and ratio approximations, Phys. Rev. C **81**, 024612 (2010).

[25] G. Potel, F. M. Nunes, and I. J. Thompson, Establishing a theory for deuteron induced surrogate reactions, Phys. Rev. C **92**, 034611 (2015).

[26] A. Ratkiewicz, J. A. Cizewski, J. E. Escher, G. Potel, J. T. Harke, R. J. Casperson, M. McCleskey, R. A. E. Austin, S. Burcher, R. O. Hughes, B. Manning, S. D. Pain, W. A. Peters, S. Rice, T. J. Ross, N. D. Scielzo, C. Shand, and K. Smith, Towards Neutron Capture on Exotic Nuclei: Demonstrating $(d, p\gamma)$as a Surrogate Reaction for (n, γ) Phys. Rev. Lett. **122**, 052502 (2019).

[27] M. Guttormsen, T. Tveter, L. Bergholt, F. Ingebretsen, and J. Rekstad, The unfolding of continuum γ-ray spectra, Nucl. Instrum. Methods Phys. Res. A **374**, 371 (1996).

[28] A. Simon, M. Guttormsen, A. C. Larsen, C. W. Beausang, P. Humby, J. T. Harke, R. J. Casperson, R. O. Hughes, T. J. Ross, J. M. Allmond, R. Chyzh, M. Dag, J. Koglin, E. McCleskey, M. McCleskey, S. Ota, and A. Saastamoinen, First observation of low-energy γ-ray enhancement in the rare-earth region, Phys. Rev. C **93**, 034303 (2016).

[29] F. Naqvi, A. Simon, M. Guttormsen, R. Schwengner, S. Frauendorf, C. S. Reingold, J. T. Harke, N. Cooper, R. O. Hughes, S. Ota, and A. Saastamoinen, Nuclear level densities and γ-ray strength functions in samarium isotopes, Phys. Rev. C **99**, 054331 (2019).

[30] A. Simon and F. Naqvi, Indirect determination of neutron-capture cross sections for Sm isotopes, Phys. Rev. C **101**, 014619 (2020).

[31] N. Otuka, E. Dupont, V. Semkova, B. Pritychenko, A. Blokhin, M. Aikawa, S. Babykina, M. Bossant, G. Chen, S. Dunaeva, R. Forrest, T. Fukahori, N. Furutachi, S. Ganesan, Z. Ge, O. Gritzay, M. Herman, S. Hlavač, K. Katō, B. Lalremruata *et al.*, Towards a more complete and accurate experimental nuclear reaction data library (EXFOR): International collaboration between nuclear reaction data centres (NRDC), Nucl. Data Sheets **120**, 272 (2014).